J. Phys. B: At. Mol. Opt. Phys. **41** (2008) 045201 (15pp) doi:10.1088/0953-4075/41/4/045201

Absolute cross sections and kinetic energy release distributions for electron-impact dissociative excitation and ionization of NeD^+

J Lecointre[1], J J Jureta[1,2], J B A Mitchell[3], V Ngassam[4], A E Orel[4] and P Defrance[1]

[1] Université Catholique de Louvain, Département de Physique, unité PAMO, Chemin du Cyclotron 2, B-1348 Louvain-la-Neuve, Belgium
[2] Institute of Physics, PO Box 68, 11081, Belgrade, Serbia
[3] PALMS, 'Equipe d'astrochimie expérimentale', UMR N°6627 du CNRS, Université de Rennes I, F-35042 Rennes, France
[4] Department of Applied Science, University of California, Davis, CA 95616, USA

Received 31 August 2007, in final form 10 December 2007
Published 11 February 2008
Online at stacks.iop.org/JPhysB/41/045201

Abstract
Absolute cross sections for electron impact dissociative excitation and ionization of NeD^+ leading to the formation of singly and multiply charged products (D^+, Ne^+, Ne^{2+} and Ne^{3+}) are reported, in the energy range from their respective thresholds to 2.5 keV. The animated crossed-beams method is used. For singly charged fragments, absolute cross sections are obtained separately for dissociative excitation and for dissociative ionization. Dissociative excitation is seen to be restricted to the low-energy range (<300 eV) and the D^+ formation dominates over the Ne^+ one. At the maximum (around 35 eV), absolute cross sections for dissociative excitation are found to be $(3.6 \pm 0.8) \times 10^{-17}$ cm^2 and $(6.3 \pm 1.4) \times 10^{-17}$ cm^2 for Ne^+ and D^+, respectively; the corresponding appearance energies are (9.1 ± 0.5) eV and (10.0 ± 0.5) eV. The absolute cross section for dissociative ionization (Ne^++D^+ formation) is found to be $(7.1 \pm 1.4) \times 10^{-17}$ cm^2, around 155 eV, and the threshold energy is (26.8 ± 0.5) eV. For multiply charged products, absolute cross sections are found, around the maximum, to be $(5.4 \pm 0.5) \times 10^{-18}$ cm^2 and $(18.2 \pm 2.6) \times 10^{-20}$ cm^2 for Ne^{2+} and Ne^{3+}, respectively; the corresponding thresholds are (53.1 ± 1.0) eV and (132 ± 5) eV. Kinetic energy release distributions are determined for each detected ionic product. The presented potential energy curves correspond to dissociation channels, which are significant for the discussion of present results. At fixed electron energy, the cross sections for the various ionization channels are seen to decrease exponentially with the potential energy of each dissociated ion pair.

1. Introduction

Rare gas hydride ions (HeH^+, NeH^+, ArH^+) were first observed in mass spectrometers around 1933 (Lukanow and Schuetze 1933, Bainbridge 1933). Ion–molecule reactions involving hydrogen or deuterium and noble gas atoms are of great interest in many types of plasma. In particular, for the future thermonuclear reactor, neon gas is envisaged as a way of cooling the hot plasma in the divertor region to avoid wall destruction. Reactions of neon gas with vibrationally excited H_2^+ lead to formation of NeH^+ molecular ions, which also play a role in plasma chemistry (Mitchell 1996, 2001). In this context, interactions with electrons are of major importance, as they are known to be responsible for the destruction of the molecular bond via recombination (dissociative recombination, DR), excitation (dissociative excitation, DE) or ionization (dissociative ionization, DI). Thus, absolute cross sections

for electron impact dissociative processes are of particular interest.

NeH^+ ions are formed in low concentration, which makes the experimental measurement of their properties quite difficult. Among the first experimental investigations, inelastic loss measurements were performed for NeH^+ (and NeD^+) colliding on noble gas target atoms (He, Ar and Kr). The analysis of the velocity distributions observed for the dissociation fragments (Schopman and Los 1971) leads to three conclusions. First, the primary beam contains a fraction of molecular ions formed in the lowest excited singlet or triplet state; next, the main dissociation mechanism is due to vibrational excitation by polarization forces and finally, at large scattering angles, excitation of the target atom dominantly contributes to the dissociation process.

Recently, Mitchell *et al* (2005) and Novotny (2006) studied dissociative recombination of NeH^+ ions with low-energy electrons. This experiment was performed by using the electron–ion merged beams technique at the heavy-ion storage ring (ASTRID) located at the University of Aarhus, Denmark. The ions are produced from a 50/50 hydrogen/neon mixture in an electron impact source, injected into the ring and accelerated to 2.5 MeV. The ion beam is merged over 0.95 m with an electron beam of known energy, formed in the electron cooler assembly. These authors established that the measured relative cross section also reflects neutral formation via dissociative excitation above about 10 eV. Consequently, the large signal, which appears in the electron energy range of interest to fusion divertor plasmas, seems to indicate that molecular ions will be dissociated, with a high probability, via neutralization or electronic excitation. Preliminary calculations, included in the paper, support this analysis. Rovibrational lifetimes have also been evaluated; they were found to lie around a few milliseconds, within the electronic ground state of NeH^+.

Ab initio potential energy curves calculations have been carried out for NeH^+, mainly for the ground electronic state ($X^1\Sigma^+$) (e.g., Peyerimhoff 1965, Bondybey *et al* 1972, Vasudevan 1975 and Rosmus and Reinsch 1980). Potential energy curves for excited states of the NeH^+ ion were obtained by Ngassam *et al* (2007). Petsalakis *et al* (1998) studied potential energy curves and vibrational levels for Rydberg states of NeH and NeD.

The present paper concerns the production of ionic species from the NeD^+ diatomic molecular ion by electron impact. Under the Born–Oppenheimer approximation and disregarding vibrational excitation, the energies as well as the lifetimes of the electronic states of NeD^+ are identical to those of NeH^+. Therefore, the deuterated target NeD^+ is chosen rather than NeH^+ to make easier the collection of the fragments. Each singly charged ion, detected separately, might arise from one of the two dissociative excitation channels (1) or (2) and also from the dissociative ionization reaction (3), above the ionization threshold. Processes leading to the formation of doubly and triply charged ions are studied via reactions (4) and (5):

$$NeD^+ + e^- \rightarrow Ne^+ + D + e^- \qquad \sigma_1 \qquad (1)$$

$$\rightarrow Ne + D^+ + e^- \qquad \sigma_2 \qquad (2)$$

$$NeD^+ + e^- \rightarrow (NeD^{2+})^* + 2e^-$$

$$\rightarrow Ne^+ + D^+ + 2e^- \qquad \sigma_3 \qquad (3)$$

$$\rightarrow Ne^{2+} + \ldots \qquad \sigma_4 \qquad (4)$$

$$\rightarrow Ne^{3+} + \ldots \qquad \sigma_5. \qquad (5)$$

In the present paper, absolute cross sections are reported for the excitation channels (1) and (2) and for the ionization channels (3)–(5), from their respective threshold up to 2.5 keV. The doubly charged NeD^{2+} ions are formed in excited states (designated by *) which are not stable; their lifetime is much smaller than their time of flight from the collision region to the detector (a few microseconds) and they preferentially dissociate into the singly charged ion pair. The direct Ne^+ and D^+ ion production measurements correspond to the sum of the dissociative excitation and the ionization processes ($\sigma_{1.3} = \sigma_1 + \sigma_3$ and $\sigma_{2.3} = \sigma_2 + \sigma_3$, for Ne^+ and D^+, respectively). A specific procedure was developed to estimate σ_1, σ_2 and σ_3, separately, which is described later in this paper. Concerning the multiply charged products Ne^{2+} and Ne^{3+}, only the total absolute cross sections (σ_4 and σ_5) are discussed here, without attempting to detail the eventual individual contributing processes.

In the second section, the experimental set-up and the data analysis method are briefly recalled for the estimation of (i) absolute cross sections and (ii) kinetic energy release distributions (KERDs). Potential energy curves, corresponding to dissociation channels, which are significant for the discussion of the present results, are presented in the third section. The last section of this paper is devoted to the description and the discussion of the results obtained for reactions (1)–(5).

2. Theoretical calculations for NeH, NeH^+ and NeH^{2+}

Potential energy curves, corresponding to dissociation channels, which are useful for the present discussion, are presented in the next section. Several theoretical investigations were carried out for the structure of NeH and NeH^+ molecules, including electronic and vibrational excited states (for instance, see Peyerimhoff 1965, Bondybey *et al* 1972, Vasudevan 1975, Rosmus and Reinsch 1980, Petsalakis *et al* 1998 and Ngassam *et al* 2007). Potential energy curves corresponding to dissociation channels (*a*)–(*i*) which are relevant for the discussion of the present results are based on those theoretical works. Dissociation limits corresponding to excited and ionized H or Ne atoms are deduced from Bashkin and Stoner (1975):

$$NeH(1\sigma^2 2\sigma^2 3\sigma^2 4\sigma 1\pi^4, X^2\Sigma^+) \rightarrow Ne(1s^2 2s^2 2p^6, {}^1S) + H(1s, {}^2S) \qquad (a)$$

$$NeH(1\sigma^2 2\sigma^2 3\sigma^2 5\sigma 1\pi^4, A^2\Sigma^+) \rightarrow Ne(1s^2 2s^2 2p^6, {}^1S) + H^*(2s, {}^2S) \qquad (b)$$

$$NeH^+(1\sigma^2 2\sigma^2 3\sigma^2 1\pi^4, X^1\Sigma^+) \rightarrow Ne(1s^2 2s^2 2p^6, {}^1S) + H^+ \quad (c)$$

$$NeH^+(1\sigma^2 2\sigma^2 3\sigma 1\pi^4 4\sigma, a^3\Sigma^+, B^1\Sigma^+) \rightarrow Ne^+(1s^2 2s^2 2p^5, {}^2P) + H(1s, {}^2S) \quad (d)$$

$$NeH^+(1\sigma^2 2\sigma^2 3\sigma^2 1\pi^3 4\sigma, b^3\Pi, A^1\Pi) \rightarrow Ne^+(1s^2 2s^2 2p^5, {}^2P) + H(1s, {}^2S) \quad (e)$$

$$NeH^+(1\sigma^2 2\sigma^2 3\sigma 1\pi^4 2\pi, d^3\Pi, D^1\Pi) \rightarrow Ne^+(1s^2 2s^2 2p^5, {}^2P) + H^*(2s, {}^2S) \quad (f)$$

$$NeH^+(1\sigma^2 2\sigma^2 3\sigma^2 1\pi^2 2\pi^2, e^3\Sigma^+, E^1\Sigma^+) \rightarrow Ne^+(1s^2 2s^2 2p^5, {}^2P) + H^*(2s, {}^2S) \quad (g)$$

$$NeH^+(1\sigma^2 2\sigma 3\sigma^2 1\pi^4 4\sigma, c^3\Sigma^+, C^1\Sigma^+) \rightarrow Ne^*(1s^2 2s 2p^5 3s, {}^{1,3}P) + H^+ \quad (h)$$

$$NeH^{2+}(1\sigma^2 2\sigma^2 3\sigma^2 1\pi^3, X^2\Pi) \rightarrow Ne^+(1s^2 2s^2 2p^5, {}^2P) + H^+. \quad (i)$$

Potential energy curves are represented in figures 1(a) and (b), for the NeH^+ singlet and triplet states, respectively. Some important potential energy curves are shown for NeH, NeH^{**} and NeH^{2+} in both these figures. Electron-scattering calculations using the complex Kohn variational methods are used to produce the potential energy curves of the resonant states as well as the autoionization width at a small internuclear distance. This method has been fully described elsewhere (see Rescigno *et al* (1995b); and references therein). Standard molecular structure calculations are used to describe NeH^+ ion states (Rescigno *et al* 1995a). Self-consistent-field (SCF) calculation is carried out on the NeH^+ ion to produce a set of molecular orbitals. Neon and hydrogen are described using a triple-zeta-plus-polarization (TZP) basis. These orbitals are then used in an all singles and doubles configuration-interaction (CI) calculation to obtain the ground and excited states of NeH^+ (Ngassam *et al* 2007). Existing calculations were reviewed by Rescigno *et al* (1995a) and, to the author's knowledge, no fundamental improvement has been achieved since then.

The NeH ground state $X^2\Sigma^+$ (*a*) is unstable, whereas the excited one $A^2\Sigma^+$ (*b*) is metastable, its lifetime being shorter than 6 ns and 0.4 μs for NeH and for NeD, respectively (Petsalakis *et al* 1998).

The ground state configuration of the NeH^+ molecular ion is $(1\sigma)^2(2\sigma)^2(3\sigma)^2(1\pi)^4$. The NeH^+ ground state $X^1\Sigma^+$ (*c*) is stable and it is the only singly charged ion state to exhibit a large potential depth. This state dissociates to the $Ne(1s^2 2s^2 2p^6, {}^1S)+H^+$ atomic limit. For NeH^+ (channels (*c*)–(*h*)), most of the potential curves correspond to charge–exchange reactions (Ne^++H) and only channel (*h*) leads to the formation of a proton (Ne^*+H^+). The first excited state configuration of the NeH^+ molecular ion is $(1\sigma)^2(2\sigma)^2(3\sigma)^2(1\pi)^3(4\sigma)^1$. The lowest excited states ($a^3\Sigma^+$, $b^3\Pi$, $A^1\Pi$ and $B^1\Sigma^+$) are mutually close at the NeH^+ equilibrium distance and they lead to the $Ne^+(1s^2 2s^2 2p^5, {}^2P)+H(1s, {}^2S)$ final configuration. Among these, the $C^1\Sigma^+$ and the $c^3\Sigma^+$ states, which nearly coincide with each other, are the lowest dissociating states allowing H^+ formation. The highest calculated molecular states all lead to the formation of Ne^+ plus an excited hydrogen atom. The $E^1\Sigma^+$ and the $e^3\Sigma^+$ states almost overlap, while the $D^1\Pi$ and the $d^3\Pi$ states, as well as the $F^1\Pi$ and the $f^3\Pi$ states, are nearly degenerated. Finally, a state corresponds to the formation of the excited neon ion $Ne^{*+}(1s^2 2s 2p^6, {}^2S)$ and to the H(1s, ^{2}S) atom. The related theoretical $g^3\Sigma^+$ state is still undetermined but, tentatively, for the present discussion, its shape is assumed identical to the calculated $a^3\Sigma^+$ one. As NeH^{2+} and HF^+ molecular ions are isoelectronic, the corresponding ground state is assigned to be $X^2\Pi$ (Bondybey *et al* 1972), which leads to ion pair formation (*i*). It is thus represented by a pure coulombic repulsive potential energy curve.

Curves representing dissociative Rydberg states of NeH^{**}, calculated by Florescu-Mitchell and Orel (2004), are included between the ground state $X^1\Sigma^+$ and the first excited state $a^3\Sigma^+$ of NeH^+ (figure 1(b)). The influence of these states on the threshold for dissociative excitation will be discussed in section 3.4. Note that electronic states with the same symmetry and multiplicity may give rise to avoided crossings, which could make difficult the unequivocal assignment of atomic dissociation limits.

The NeH^+ equilibrium distance (r_e) is estimated to be 1.83 au by Peyerimhoff (1965) and Vasudevan (1975); this is found to be smaller than the value (1.85 au) of Bondybey *et al* (1972). Moreover, Petsalakis *et al* (1998) and Ngassam *et al* (2007) agree together as both of them evaluated the equilibrium distance to be 1.895 au. All these theoretical data stay reasonably close to the measurements of Weise *et al* (1971) (1.87 au) and Rich *et al* (1971) (1.90 au). Petsalakis *et al* (1998) calculated the theoretical dissociation energy (D_0) to be 2.11 eV which agrees with the experimental values of Berkowitz (1971) (2.08 $\pm$ 0.03 eV) and that of Lorenzen *et al* (1980) (2.10 $\pm$ 0.03 eV). These data are also found to be similar to the predictions of Bondybey *et al* (1972) (2.10 eV) and of Vasudevan (1975) (2.13 eV). Peyerimhoff (1965) and Ngassam *et al* (2007) calculated the theoretical dissociation energy to be 2.21 eV and 2.32 eV, respectively, which is somewhat higher than all the above-mentioned results. Additionally, the lifetimes of rovibrational levels of the $X^1\Sigma^+$ state of NeH^+ were estimated to lie between 0.8 and 2.8 ms (Mitchell *et al* 2005).

3. Apparatus and experimental method

In this experiment, the animated crossed electron–ion beam method is applied (Defrance *et al* 1981). Both the present apparatus and the experimental method have recently been described in detail (Lecointre *et al* 2006) and only a brief outline is presented here.

3.1. Experimental set-up

In the apparatus, the fixed-energy molecular ion beam interacts at right angles, with an electron beam whose energy may be tuned from a few electron-Volts up to 2.5 keV. Ions are

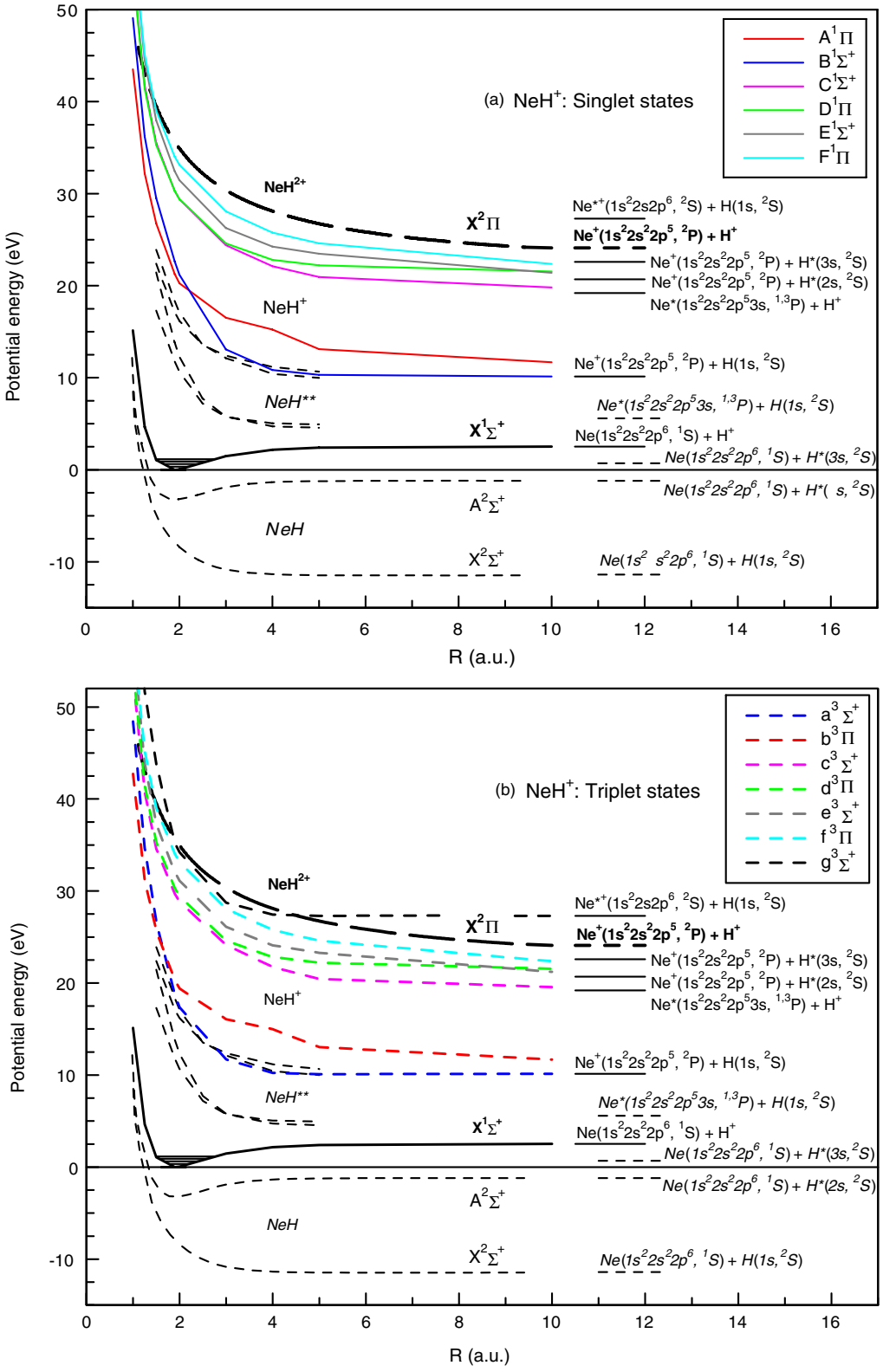

Figure 1. (a) Potential energy curves for NeH, NeH^+ singlet states and NeH^{2+}. (b) Potential energy curves for NeH, NeH^+ triplet states and NeH^{2+}.

Note: both figures 1(a) and (b) are deduced from Bondybey *et al* (1972), Vasudevan (1975), Bashkin and Stoner (1975), Rosmus and Reinsch (1980), Petsalakis *et al* (1998), Florescu-Mitchell and Orel (2004) and Ngassam *et al* (2007). For details, see text.

(This figure is in colour only in the electronic version)

extracted from an ECR ion source and accelerated to 12 keV. The NeD^+ molecular ion is obtained by mixing neon and deuterium in the ion source, around 10% of Ne and 90% of D_2. The pressure in the ECR ion source is 7×10^{-3} mbar and the microwave power is around 100 W. The ion beam is selected by means of a first double focusing 90° magnetic analyser, additionally focused and purified by a 45° spherical electrostatic deflector, and directed into the collision region where it crosses the ribbon-shaped electron beam, at right angles. Product ions are separated from the primary ion beam by means of a second double focusing 90° magnetic analyser. Due to the transfer of internal potential energy, dissociation fragments exhibit both a broad velocity and a broad angular distribution in the laboratory frame. Selected by the variable analyser slit, the angular acceptance of the magnet (0.1 radian) is large enough to transmit all ions to the detector with the maximum expected kinetic energy release produced by dissociation processes. Product ions are further deflected by a 90° electrostatic spherical deflector and directed onto a channeltron detector.

3.2. Cross-section measurements

In the animated beam method (Defrance *et al* 1981), the electron beam is swept across the ion beam in a linear motion at a constant speed u. The total number of events K produced during one complete electron beam movement is related to the cross section σ by the following expression:

$$\sigma = \frac{uK}{AI_eI_i\gamma}, \tag{6}$$

where γ is the detector efficiency, I_e and I_i are the electron and ion beam current intensities, respectively, and A, a kinematic factor, which for beams interacting at a right angle, is given by

$$A = \frac{\left(v_e^2 + v_i^2\right)^{1/2}}{v_e v_i q_i e^2}. \tag{7}$$

In this expression, e and q_ie, v_e and v_i, are the charges and velocities of electrons and ions, respectively. Assuming $m_i \gg m_e$, the true interaction energy E (eV) is given by

$$E = V_e + \frac{m_e}{m_i}(q_iV_i - V_e), \tag{8}$$

where v_e and v_i, m_e and m_i are the acceleration voltages and masses of electrons and target ions, respectively. The electron energy is corrected for contact potentials, by measuring accurately the appearance potential for well-known physical processes, such as single ionization of noble gas ions, Ar^+ or Ne^+.

3.3. Total cross-sections and kinetic energy release distributions

The angular acceptance of the magnet analyser allows the total transmission of the angular distribution of product fragments emitted at a given velocity v in the laboratory frame. This velocity is defined by the magnetic field B ($v = qRB/m$) and is also given by $\sqrt{v_c^2 + w^2 + 2v_cw\cos\theta_L}$, where v_c, θ_L and w represent the centre-of-mass velocity, the ejection angle in the laboratory and the fragment velocity in the centre-of-mass frame, respectively. Here, m and q are the fragment ion mass and charge, and R is the radius of its trajectory in the analyser magnetic field.

Due to the KER, the velocity distribution ($f(v) = \mathrm{d}\sigma(v)/\mathrm{d}v$) usually exceeds the corresponding magnetic analyser acceptance, which is essentially defined by the size of the analysing slits. Consequently, the total transmission of dissociation products to the detector cannot be achieved. In order to put the cross section on the absolute scale, the velocity distribution must be determined and integrated over the full velocity range. For this purpose, first, the apparent cross section $\sigma_m(B)$ is measured at a given electron energy as a function of the analyser magnetic field (B). Next, the corresponding differential cross section, $(\mathrm{d}\sigma(B)/\mathrm{d}B)$, is computed (Lecointre *et al* 2006) from which the velocity distribution is obtained as

$$f(v) = \frac{\mathrm{d}\sigma(v)}{\mathrm{d}v} = \frac{m}{qR}\frac{\mathrm{d}\sigma(B)}{\mathrm{d}B}. \tag{9}$$

The total cross section σ is obtained by integrating this distribution over the entire velocity range:

$$\sigma = \int_0^\infty f(v)\,\mathrm{d}v. \tag{10}$$

It was demonstrated (Lecointre *et al* 2006) that the total kinetic energy release distribution (KERD), for the investigated fragment, may be expressed in terms of the velocity distribution by

$$\frac{\mathrm{d}\sigma\,(E_{\mathrm{KER}})}{\mathrm{d}E_{\mathrm{KER}}} = \frac{-2\mu v_c}{m^2\,(1-\varepsilon/2)}\frac{\mathrm{d}}{\mathrm{d}v}\left(\frac{1}{v}\frac{\mathrm{d}\sigma\,(v)}{\mathrm{d}v}\right), \tag{11}$$

where μ is the reduced mass of the fragments. In the present experiment, ε is expressed as

$$\varepsilon = 2\left(1 - \frac{2v_c}{\sigma}\int_{v_c}^\infty \frac{1}{v}\frac{\mathrm{d}\sigma(v)}{\mathrm{d}v}\,\mathrm{d}v\right). \tag{12}$$

This quantity was seen to characterize the angular distribution of dissociation products with respect to the velocity of the incident electron, due to the initial orientation of the molecular axis. E_{KER} represents the sum of the kinetic energy released to the dissociation fragments. By assuming the fragmentation of the target to be binary only and by applying the momentum conservation, this sum is given by

$$E_{\mathrm{KER}} = \frac{m^2w^2}{2\mu}. \tag{13}$$

3.4. Experimental procedure

As described above, at a fixed v, only a fraction η of the fragment velocity distribution is detected at once. To overcome this problem, the above-mentioned magnetic field scans are performed at fixed electron energies. The repetition of this procedure at each electron energy results in a very long and tedious task. In order to reduce it with little effect on the accuracy of final results, an alternative procedure (Bahati *et al* 2001) was introduced to cover the whole energy range without measuring all the distributions. In the first step, the apparent cross section $\sigma_m(B_0)$ is measured versus the electron energy at the magnetic field B_0 which corresponds to the centre of the

velocity distribution, that is to the detection of fragments with $v = v_c$. Working at this field is necessary in order to include the contributions of all the ejection speeds in the centre-of-mass frame. The absolute cross section is related to the apparent one by

$$\sigma = \sigma_m(B_0)/\eta. \tag{14}$$

To put the apparent cross section $\sigma_m(B_0)$ on the absolute scale over the whole electron energy range, the transmission factor is first computed at the selected electron energies where magnetic field scans are performed. Five energies are generally selected, ranging from the reaction threshold up to 300 eV while above this energy, the transmission factor was seen to be constant (Lecointre *et al* 2006). Next, these results are interpolated and extrapolated in order to estimate η at any electron energy and the apparent cross section is corrected by means of (14) to obtain the absolute cross section.

3.5. Separation of DE and DI (Ne^+ and D^+)

Products of reactions (1) and (3) for Ne^+ as well as (2) and (3) for D^+ form two velocity distributions whose shapes depend on the electron energy, i.e. on the various involved E_{KERs}. At low energies, below the ionization threshold, only dissociative excitation is observed. The width of the spectra is seen to increase significantly with the electron energy, because of the larger kinetic energy released to the fragments, associated with the opening of new possible reaction channels. Above the ionization threshold, the spectrum is broader, due to Coulomb repulsion experienced by DI fragments. In the experiment, magnetic field scans were recorded at several specific incident electron energies. The spectra exhibit a change of slope that indicates the presence of the two distinct dissociative contributions. The upper part (the narrow one) of the distribution corresponds to DE (reactions (1) and (2), low KER) and the lower part (the wider one) is attributed to DI (reaction (3), large KER). This is illustrated for the D^+ production in figure 7(b), where the two dissociative contributions are clearly discernable in the kinetic energy release distributions.

The dissociative ionization signal is isolated by fitting the outer part of the spectrum. The apparent cross section versus the electron energy $\sigma_m^{DI}(E)$ is measured at a fixed magnetic field, high enough to avoid the DE contribution (Lecointre *et al* 2006 and Cherkani-Hassani *et al* 2006). Consequently the pure DI contribution is obtained and the transmission factor $\eta_{DI}(E)$ is calculated at this high magnetic field to put the apparent cross section on an absolute scale by means of the expression:

$$\sigma_3(E) = \frac{\sigma_m^{DI}(E)}{\eta_{DI}(E)}. \tag{15}$$

Absolute values of DE cross sections (σ_1 or σ_2, for Ne^+ and D^+, respectively) are obtained by subtracting the DI contribution (σ_3) from the total absolute cross section ($\sigma_{1.3}$ or $\sigma_{2.3}$, for Ne^+ and D^+, respectively).

3.6. Experimental conditions

Present measurements concern absolute total cross sections for production of Ne^+ ($\sigma_{1.3}$), D^+ ($\sigma_{2.3}$), Ne^{2+} (σ_4) and Ne^{3+} (σ_5). For singly charged fragments, the analysis of the experimental results provides us with individual DE and DI contributions (σ_1, σ_2 and σ_3). For each ion, KERDs are determined at selected electron energies where magnetic field scans were performed.

Typical working conditions are the following: primary NeD^+ ion current 1–2 nA; electron current 0.5–2.5 mA; electron beam sweeping speed 3.75 m s^{-1}. The number of events per sweep is 0.2–0.5 for both Ne^+ and D^+ fragments and it is found to be 9×10^{-3} and 6×10^{-4}, for Ne^{2+} and Ne^{3+} products, respectively. In order to reduce the background, the pressure is kept below 1×10^{-9} mbar in the collision chamber during the measurement.

Transmission factors (η) are determined directly from each measured magnetic field distribution (equation (14)). They range from 57% at low electron energies to about 36% at high electron energies for Ne^+ and from 21% to 12% for D^+. For Ne^{2+}, transmission factors range from 65% to about 53%, whereas for Ne^{3+}, they lie around 34%. The transmission factor is directly linked to the width of the velocity distribution: close to the threshold, it tends towards the maximum; for high energies, it is lowered since the velocity distribution becomes wider and, above 100 eV, it is seen to reach a constant value.

The uncertainty associated with the transmission factor is estimated to be 5%. The total uncertainty (90% confidence limit) is obtained as the square root of the quadratic sum of the statistical and systematic uncertainties. Systematic uncertainties affecting the cross section (equation (6)) are ±1% for the detector efficiency (γ), ±1% for the sweeping speed (u), ±0.5% for both the electron (I_e) and ion (I_i) beam current intensities and ±0.5% for the kinematic factor (A) (Lecointre *et al* 2006). The total uncertainty is found to be 10.0%, 9.0%, 9.4% and 12.0% for $\sigma_{1.3}$, $\sigma_{2.3}$, σ_4 and σ_5, respectively, at the cross-section maximum. Moreover, the uncertainty associated with the fitting procedure is estimated to be 10% so that the total uncertainty (90% confidence limit) is found to be 22%, 21% and 19% for σ_1, σ_2 and σ_3, respectively. The uncertainty associated with the electron energy is estimated to be ±0.5 eV (Lecointre *et al* 2006).

4. Results and discussion

The following sections are dedicated to the description and the discussion of the results (threshold energies, absolute cross sections and kinetic energy release distributions) which are obtained for reactions (1)–(5).

For singly charged fragments, absolute cross sections are listed in table 1 ($\sigma_{1.3}$, $\sigma_{2.3}$, σ_1, σ_2 and σ_3) together with associated total uncertainties. For reactions (1)–(3), table 2 lists the experimentally observed threshold energies and E_{KERs} together with theoretical results and table 4 shows the present mean kinetic energy release values ($\overline{E_{KER}}$). Experimental KER ranges and corresponding mean values ($\overline{E_{KER}}$) are deduced from the analysis of observed kinetic energy release distributions (KERDs).

Table 1. Absolute cross sections for the total production of Ne^+ and D^+, for DE and for DI (10^{-17} cm^2, 90% confidence limit).

	Total $\sigma_{1.3}$: Ne^+		Total $\sigma_{2.3}$: D^+		DE σ_1: Ne^+		DE σ_2: D^+		DI σ_3: $Ne^+ + D^+$	
E (eV)	$\sigma_{1.3}$	$\Delta\sigma_{1.3}$	$\sigma_{2.3}$	$\Delta\sigma_{2.3}$	σ_1	$\Delta\sigma_1$	σ_2	$\Delta\sigma_2$	σ_3	$\Delta\sigma_3$
9.1	0.0	0.1	−0.02	0.05	0.0	0.1	−0.02	0.05		
10.1	0.2	0.1	0.03	0.05	0.2	0.1	0.03	0.05		
11.1	0.4	0.1	0.3	0.2	0.4	0.1	0.3	0.2		
12.1			0.5	0.1			0.5	0.1		
13.1	0.6	0.1	0.7	0.1	0.6	0.1	0.7	0.1		
14.1			1.2	0.2			1.2	0.2		
15.1	1.2	0.2	1.6	0.1	1.2	0.2	1.6	0.1		
17.1	1.7	0.2	2.6	0.3	1.7	0.2	2.6	0.3		
19.1			3.3	0.4			3.3	0.4		
21.1	2.5	0.1	4.2	0.4	2.5	0.3	4.2	1.0	0.0	0.1
23.1			4.9	0.5			4.6	1.0	0.3	0.1
25.1	3.0	0.3	5.5	0.1	2.8	0.7	5.3	0.4	0.2	0.2
27.1									0.1	0.1
30.1	3.7	0.4	6.4	0.6	3.2	0.8	5.9	1.3	0.5	0.2
31.1									0.5	0.2
33.1									0.8	0.2
35.1	4.5	0.5	7.2	0.7	3.6	0.8	6.3	1.4	0.9	0.3
40.1	5.1	0.5	8.0	0.7	3.4	0.8	6.3	1.4	1.7	0.4
45.1	5.4	0.2	8.4	0.2	2.9	0.3	5.9	0.3	2.5	0.3
55.1	6.1	0.6	9.0	0.8	2.4	0.6	5.3	1.2	3.7	0.8
65.1	6.6	0.7	9.8	0.9	1.8	0.6	5.0	1.1	4.8	1.0
75.1	7.1	0.7	10.3	1.0	1.8	0.7	5.1	1.2	5.3	1.1
85.1	7.5	0.8	10.8	1.0	1.6	0.6	4.9	1.1	5.9	1.2
95.1	7.7	0.2	10.9	0.2	1.4	0.2	4.6	0.6	6.3	0.6
115.1	7.9	0.8	10.9	1.0	1.0	0.6	4.1	1.1	6.8	1.4
135.1	7.7	0.8	10.9	1.0	0.7	0.4	3.8	1.0	7.0	1.4
155.1	7.5	0.8	10.0	0.9	0.6	0.5	3.1	0.8	7.1	1.4
195.1	7.0	0.7	9.5	0.9	0.0	0.3	2.6	0.7	7.0	1.3
245.1	6.6	0.7	8.4	0.8	0.0	0.5	1.4	0.6	6.8	1.4
295.1	6.2	0.2	7.5	0.2	0.0	0.2	0.9	0.5	6.6	0.7
395.1	5.5	0.6	6.5	0.6	0.0	0.2	0.8	0.3	5.7	1.1
495.1	5.0	0.5	5.8	0.6	0.2	0.2	0.9	0.3	4.9	0.9
595.1	4.5	0.5	5.1	0.5	0.2	0.2	0.8	0.3	4.3	0.8
795.1	3.8	0.4	4.2	0.4	0.3	0.2	0.6	0.2	3.5	0.7
995.1	3.4	0.4	3.6	0.4	0.4	0.2	0.5	0.3	3.1	0.6
1495.1	2.6	0.3	2.8	0.3	0.3	0.2	0.5	0.2	2.3	0.4
1995.1	2.1	0.2	2.2	0.2	0.3	0.2	0.4	0.2	1.8	0.4
2495.1	1.9	0.2	2.0	0.2	0.3	0.2	0.5	0.2	1.5	0.3

Absolute total cross sections for Ne^+ and D^+ production are shown in figures 2(a) and (b), respectively. The present maximum total cross sections are found to be $(7.9 \pm 0.8) \times 10^{-17}$ cm^2 and $(10.9 \pm 1.0) \times 10^{-17}$ cm^2 for Ne^+ ($\sigma_{1.3}$) and D^+ ($\sigma_{2.3}$), respectively.

4.1. Dissociative ionization, Ne^++D^+ formation

Attempts to observe single ionization (NeD^{2+} ions) were not successful and the corresponding cross section has been estimated to be smaller than 10^{-22} cm^2. Both products (Ne^+ and D^+) of the dissociative ionization reaction (3) provide us with two independent estimations of σ_3 that were found to agree with each other within ±15%. Present results for σ_3 are obtained in the whole energy range as the average of these two sets of data (table 1 and figure 3).

Two distinct DI thresholds are observed at (26.8 ± 0.5) eV and (35.1 ± 0.5) eV, the weak signal ranging down to 21 eV being insignificant. The direct transition to the pure Coulombic repulsive $X^2\Pi$ state in the Franck–Condon region should appear above about 35.6 eV, which is consistent with the observed DI threshold. Consequently, the lowest threshold should result from an indirect process. Potential energy curves show that the $g^3\Sigma^+$ state of NeH^+ is crossing the $X^2\Pi$ state of NeH^{2+}, so that autoionization could occur for reasonably large internuclear distances and lead to the production of the ion pair (figure 1). The threshold expected for this indirect process should be slightly lower than the direct one. Accurate potential curves corresponding to these two states should bring useful information needed to discuss the present results in more detail.

The absolute cross-section maximum is found to be $(7.1 \pm 1.4) \times 10^{-17}$ cm^2 at $E = 155.1$ eV. The Bethe plot of the dissociative ionization cross sections shows that the data are well aligned along a straight line above 60 eV (figure 4). The weak deviation from the linear behaviour around 300 eV is much smaller than the error bars, so that it is assumed to be insignificant. This plot indicates that the energy dependence of the electron impact ionization cross section can adequately

Table 2. Threshold energies and KER, for singly charged fragments.

		Thresholds (eV)				E_{KER} (eV)	
$NeD^+ + e^- \rightarrow$		Present results	Theory[a]	Molecular state	Dissociation limit D_0 ($\pm$0.1 eV)[b]	Theory[a,b] ($\pm$0.2 eV)	Present range
DE	Ne^+	9.1 ± 0.5	18.8	$a^3\Sigma^+$	$Ne^+(1s^22s^22p^5, {}^2P) + H(1s, {}^2S)$	8.3	1–9 ± 1
		13.1 ± 0.5	20.3	$b^3\Pi$	(10.5)	9.8	
			21.3	$A^1\Pi$		10.8	
			22.6	$B^1\Sigma^+$		12.1	
			30.2	$d^3\Pi$	$Ne^+(1s^22s^22p^5, {}^2P) + H^*(2s, {}^2S)$	9.5	
			30.3	$D^1\Pi$	(20.7)	9.6	
			32.0	$e^3\Sigma^+$		11.3	
			32.4	$E^1\Sigma^+$		11.7	
			34.0	$F^1\Pi$		13.3	
			34.0	$f^3\Pi$		13.3	
	D^+	10.0 ± 0.5	29.7	$c^3\Sigma^+$	$Ne^*(1s^22s^22p^53s, {}^{1,3}P) + H^+$	10.5	0–3 ± 1
		14.1 ± 0.5	30.3	$C^1\Sigma^+$	(19.2)	11.1	
DI	$Ne^+ + D^+$	26.8 ± 0.5	35.6[c]	$X^2\Pi$	$Ne^+(1s^22s^22p^5, {}^2P) + H^+$	11.5	0–18 ± 2[d]
		35.1 ± 0.5			(24.1)		3–15 ± 1

[a] Ngassam *et al* (2007).
[b] Bashkin and Stoner (1975).
[c] Present value evaluated from the Coulombic repulsive potential.
[d] For DI: the upper E_{KER} range is deduced from the Ne^+ measurements, whereas the lower one is obtained from the D^+ measurements.

be represented by the usual Bethe form

$$\sigma_3 = \frac{a}{E \times I_p}\left[\ln\left(\frac{E}{I_p}\right) + b\right], \qquad (16)$$

where I_p (eV) and E (eV) represent the ionization potential and the electron energy, respectively. The straight line in figure 4 is the result of the least-square fit of the cross section according to formula (16): the fitting parameters a and b are determined to be $(27.2 \pm 0.5) \times 10^{-14}$ cm^2 eV^2 and (-0.64 ± 0.02), respectively. The Bethe energy dependence is seen to be valid well below the cross-section maximum, whereas this dependence is generally supposed to be valid in the high-energy range only. This behaviour has already been observed for a CO^+ molecular ion (Lecointre *et al* 2006).

In the high-energy range, cross sections (σ_3) may be given in the following form (e.g., Van der Wiel *et al* 1969 and Inokuti 1971), which is linked with photoionization data:

$$\sigma_3 = \frac{4\pi a_0^2 R}{E}\left[M_I^2 \cdot \ln\left(\frac{E}{R}\right) + \gamma_I \cdot \left(\frac{R}{E}\right) + C_I\right], \qquad (17)$$

where a_0 is the first Bohr radius of atomic hydrogen, R is the Rydberg energy, γ_I and C_I are two constants depending on the target (subscript I stands for ionization). The squared matrix element (M_I^2) is obtained by integrating the generalized oscillator strength for the considered process (Miller and Platzman 1957), single dissociative ionization in the present case. At sufficiently high electron energies, the second term in the bracket $(\gamma_I \cdot (R/E))$ becomes negligible. Thus the high-energy asymptotic form of (17) is seen to be an alternative form of (16), indicating that the fitting constant (a) is directly related to the generalized oscillator strength. As a result, the present value of M_I^2 for dissociation ionization (reaction (3)) is calculated to be (2.12 ± 0.05).

4.2. Dissociative excitation, $Ne^+ + D$ and $Ne + D^+$ formation

Below the dissociative ionization threshold (26.8 eV), $\sigma_{1.3}$ and $\sigma_{2.3}$ are equal to the dissociative excitation cross sections σ_1 and σ_2, respectively, as only dissociative excitation contributes to the signal. Above the dissociative ionization threshold, DE cross sections are obtained for each ion after subtraction of the DI contribution ($\sigma_1 = \sigma_{1.3} - \sigma_3$ and $\sigma_2 = \sigma_{2.3} - \sigma_3$) and the results are presented in figures 2(a) and (b). Around the maximum of the cross sections, dissociative excitation leading to the D^+ formation is seen to dominate over the Ne^+ one: these maxima are found to be $(6.3 \pm 1.4) \times 10^{-17}$ cm^2 and $(3.6 \pm 0.8) \times 10^{-17}$ cm^2 (at $E = 35.1$ eV), respectively. Finally, above 100 eV, $\sigma_{1.3}$ and $\sigma_{2.3}$ are seen to be nearly equal to σ_3, so that DE becomes almost negligible.

For Ne^+, the present threshold energies are found to be (9.1 ± 0.5) eV and (13.1 ± 0.5) eV. At the equilibrium internuclear distance ($v = 0$), the threshold is expected around 18.8 eV due to excitation from the ground state ($X^1\Sigma^+$) to the $a^3\Sigma^+$, $b^3\Pi$, $A^1\Pi$ and $B^1\Sigma^+$ states (table 2). Let us recall that, being concerned with low-energy electrons, singlet–triplet transitions are allowed. One plausible assumption for the observed lowest energy threshold is that excitation occurs from excited vibrational levels populated within the $X^1\Sigma^+$ ground state. This would contribute to enlarge the Franck–Condon region and, subsequently, lower the threshold that may become consistent with the experimental result. This would necessitate almost all vibrationally excited states of $NeD^+(v')$ to be present in the ion beam, which are formed via the endothermic charge exchange reaction:

$$D_2^+(v) + Ne \rightarrow NeD^+(v') + D. \qquad (18)$$

In a recent pulsed-field ionization–photoelectron-secondary ion coincidence experiment (PFI–PESICO), Zhang *et al*

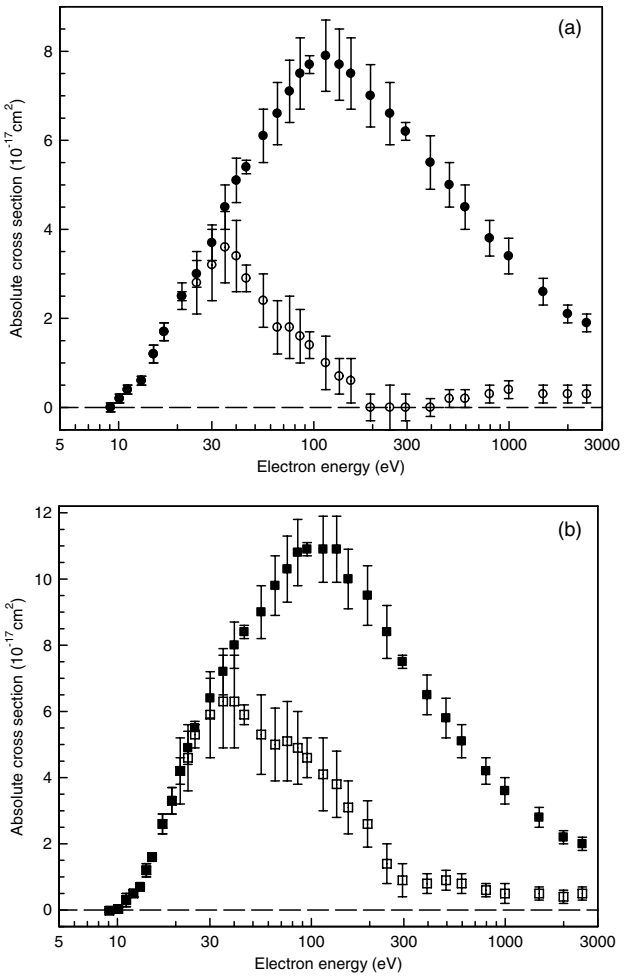

Figure 2. (a) Total absolute cross sections ($\sigma_{1,3}$; ●) and absolute cross sections for dissociative excitation (σ_1; ○) for Ne^+ fragments, versus the electron energy. (b) Total absolute cross sections ($\sigma_{2,3}$; ■) and absolute cross sections for dissociative excitation (σ_2; □) for D^+ fragments, versus the electron energy.

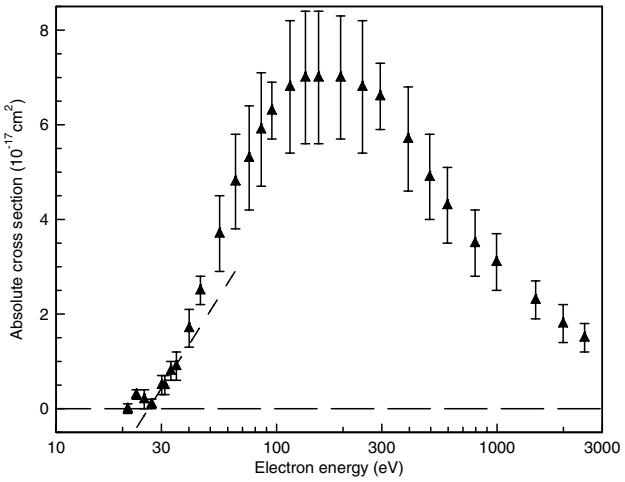

Figure 3. Absolute cross sections for dissociative ionization (σ_3; ▲), versus the electron energy. (The oblique dashed line is an eye-guide, to visualize the thresholds).

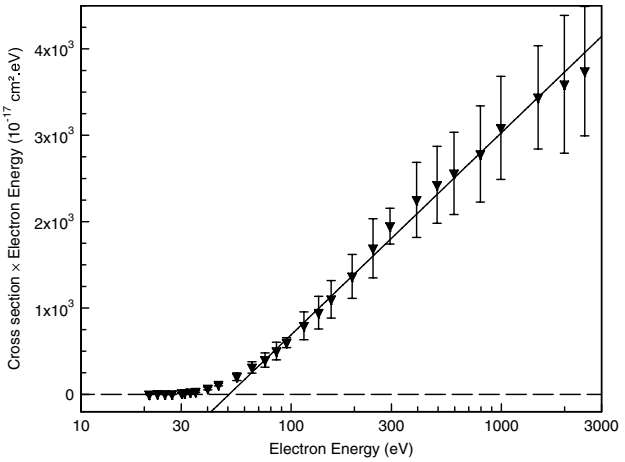

Figure 4. Bethe plot of the dissociative ionization cross section (σ_3). The full line is the result of the fit (equation (16)).

(2003) have determined cross sections for $NeH^+(v')$ formation from the individual vibrational states of $H_2^+(v)$. By combining these cross sections with a Franck–Condon vibrational population for $H_2^+(v)$ (Wind 1965), the relative importance of the $H_2^+(v)$ vibrational states to the formation of $NeH^+(v')$ is estimated (figure 5). The fact that the $v = 0$ level has a non-zero cross section is because the translational energy of the ions was 0.7 eV in this PFI–PESICO study, thus allowing the endothermic reaction to proceed.

Table 3 lists the energies of the $NeH^+(v')$ vibrational states and the exothermicities for the various vibrational levels of $H_2^+(v)$ to form $NeH^+(v')$. Available exothermicities indicate that all possible v' (<12) may be formed. The lowest neutral resonant state (also called superexcited) presents an energy which is calculated to be 10.7 eV (Florescu-Mitchell and Orel 2004), around the NeH^+ equilibrium distance. From table 3, one can deduce that to achieve a threshold of about 9 eV would require vibrational levels of $NeH^+(v')$ in excess of $v' = 6$ to be populated, assuming that isotopic effects do not induce a noticeable difference between the thresholds for NeH^+ and NeD^+. This mechanism would thus necessitate the presence of $H_2^+(v)$ levels superior to $v = 11$. Such a vibrational population is regularly observed in experiments involving H_2^+ and D_2^+ as primary ions (Abdellahi El Ghazaly *et al* 2004; and references therein). It is shown (figure 5) that this is well possible, given the fact that the NeH^+ excited vibrational states exhibit lifetimes above 0.8 ms (Mitchell *et al* 2005) which is far in excess of the transit time from the ion source to the collision region ($\sim 10^{-6}$ s).

The low experimental threshold can also be attributed to an initial capture of the electron into a doubly excited state:

$$\begin{aligned} e^- + NeD + (v') &\rightarrow (NeD)^{**} \\ &\rightarrow (NeD^+)^* + e^- \\ &\rightarrow Ne^+ + D + e^- \\ &\rightarrow Ne + D^+ + e^-. \end{aligned} \tag{19}$$

Calculations recently performed for excitation of NeD^+ (Ngassam *et al* 2007) only concern resonance-enhanced

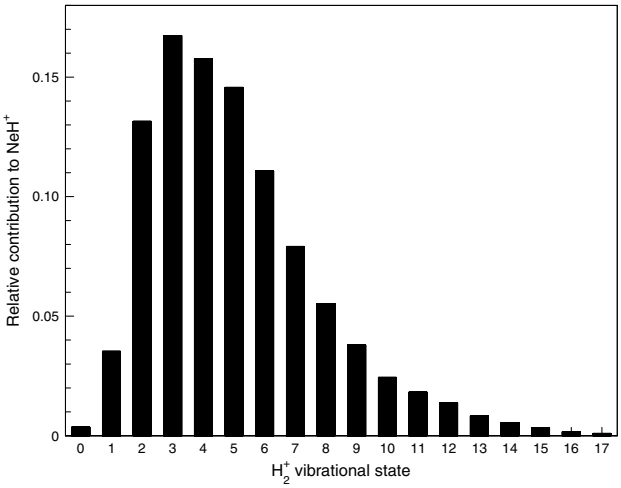

Figure 5. Relative importance of the H_2^+ vibrational states to the formation of NeH^+.

Table 3. Exothermicities of the $H_2^+(v)$ vibrational states to form $NeH^+(v')$ (reaction 18) and energies of the $NeH^+(v')$ vibrational states.

$H_2^+(v)$	Exothermicity (eV)	NeH^+ (v')	Energy (eV)
0	−0.540	0	0.000
1	−0.268	1	0.329
2	−0.013	2	0.630
3	0.228	3	0.903
4	0.454	4	1.148
5	0.665	5	1.366
6	0.862	6	1.555
7	1.045	7	1.716
8	1.215	8	1.849
9	1.371	9	1.955
10	1.512	10	2.032
11	1.648	11	2.081
12	1.754	12	2.100
13	1.852		
14	1.936		
15	2.004		
16	2.056		
17	2.090		
18	2.107		

dissociative excitation but not direct dissociative excitation. The maximum of this cross section (2.8×10^{-18} cm^2) is seen around 13 eV, which corresponds to the optimal overlap between the wavefunctions describing the ion continuum and the lowest resonant Σ state. The calculation demonstrates that the energy threshold associated with this process (8.5 eV) is close to the experimental threshold energy (9.1 eV). Finally, in addition to the above-mentioned explanations (vibrational population and resonant capture) leading to the possible low threshold, the large width of the Franck–Condon region associated with the excited vibrational levels must also be taken into account in order to explain the presence of the second threshold observed 4 eV above the lowest one.

For D^+, two threshold energies are identified at (10.0 ± 0.5) eV and (14.1 ± 0.5) eV. The lowest dissociative states ($C^1\Sigma^+$ and $c^3\Sigma^+$) accessible via direct excitation leading to

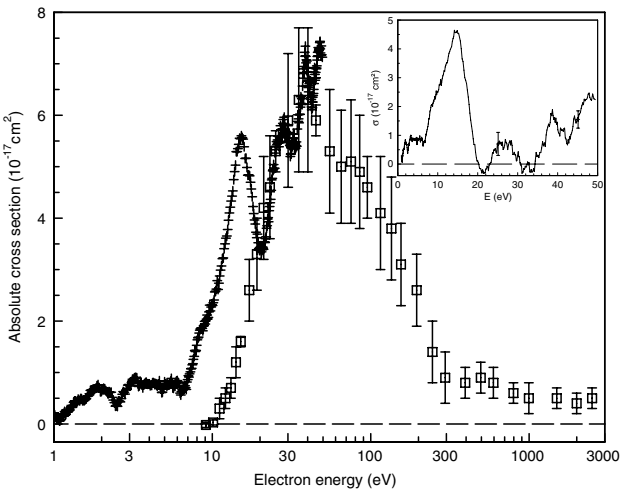

Figure 6. Absolute cross sections for dissociative excitation (reaction 2) versus electron energy: present measurements (σ_2, □) for D^+ fragments and normalized data (+) of Novotny (2006) for Ne fragments. The inset shows estimated resonant contributions. (For details, see text.)

the $Ne^*(1s^22s^22p^53s,\ ^{1,3}P) + H^+$ pair formation are shown in figures 1(a) and 1(b). The corresponding dissociation limit is high (19.2 eV) and so the threshold for dissociative excitation is much higher (29.7 eV, table 2). No theoretical result being presently available for this reaction (D^+ formation), one may presume that such low experimental thresholds are most likely due to resonant dissociative excitation (equation 19), similarly to the above-detailed discussion for Ne^+. Further calculations should enlighten the situation, as well as the role of vibrational excitation of the parent ion and of the subsequent broadening of the Franck–Condon region.

In figure 6, present absolute cross sections for dissociative excitation leading to Ne + D^+ products (σ_2) are compared with measurements performed on NeH^+ ions and obtained from an ASTRID storage ring experiment (merged beams; Novotny 2006). In that experiment, neutral Ne and Ne+H products are detected but not separately distinguished, so that the corresponding data contain both dissociative recombination and excitation contributions. Dissociative recombination, which is dominant in the low-energy range (below 1 eV), cannot be observed in the present experiment as only ions are detected. The data (figure 6) extend beyond what was originally published by Mitchell *et al* (2005). A moving average procedure with a step size of 11 points has been used to improve the statistics and this has allowed higher energy points (that had large individual statistical errors) to be included. In a storage ring measurement, the absolute ion current is difficult to measure and the calibration of the cross section measured at the ASTRID storage ring had been found to be imprecise. For this reason, the original data points measured by Mitchell *et al* (2005) were normalized to theoretical values, as the goal of that paper was to demonstrate that the DR of NeH^+ was non-negligible despite having no curve crossing through which direct dissociative recombination could proceed. The data shown in figure 6 have been normalized to the present

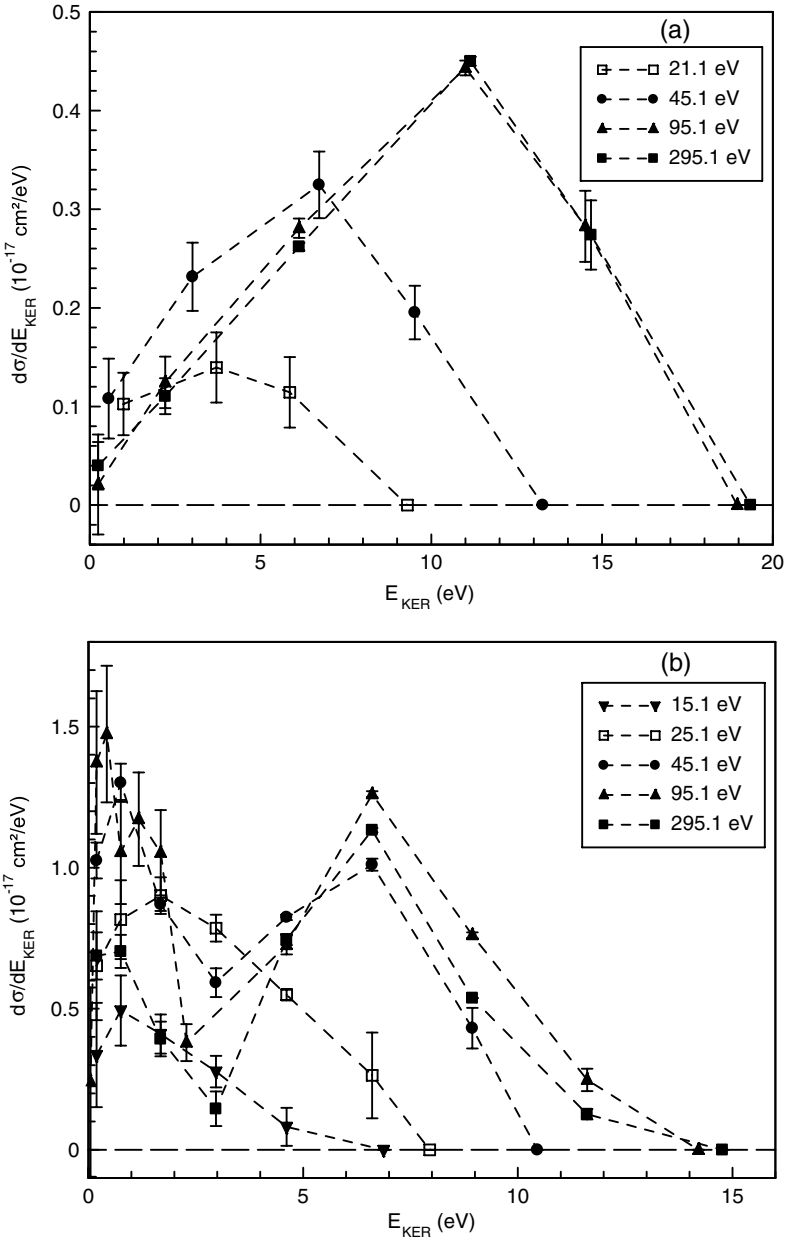

Figure 7. (a) Total kinetic energy release distributions for Ne^+ fragments, for indicated electron energies. (b) Total kinetic energy release distributions for D^+ fragments, for indicated electron energies.

absolute cross sections, at 20 eV. Several energy thresholds are observed around 7 eV, 20 eV, 33 eV and 42 eV. Below 20 eV, a distinct qualitative difference is clearly observable between the storage ring data and the present ones: the thresholds (10.0 and 14.1 eV) do not coincide with the above-listed ones and the broad peak centred on 14 eV is not seen. This is clearly a resonant contribution due to dissociative recombination, which is highlighted by subtracting the present results from the storage ring data; assuming that there will be little difference between the NeH^+ data and what one would obtain using NeD^+ ions in the storage ring (inset, figure 6). The corresponding resonant states obviously lead to formation of two neutral products (Ne+H), because no resonant signal is observed in the present experiment. One may argue that the presence of electric and magnetic fields inside the interaction region could result in amplifying the formation of neutral pairs via resonant processes. Above 20 eV both experimental results give similar overall shapes for dissociative excitation, except for the thresholds (33 eV and 42 eV), which cannot be observed in the present experiment due to larger statistical uncertainties.

4.3. Kinetic energy release distributions for Ne^+ and D^+

The theoretical KER (Ngassam *et al* 2007, Bashkin and Stoner 1975, table 2) is estimated in the Franck–Condon region

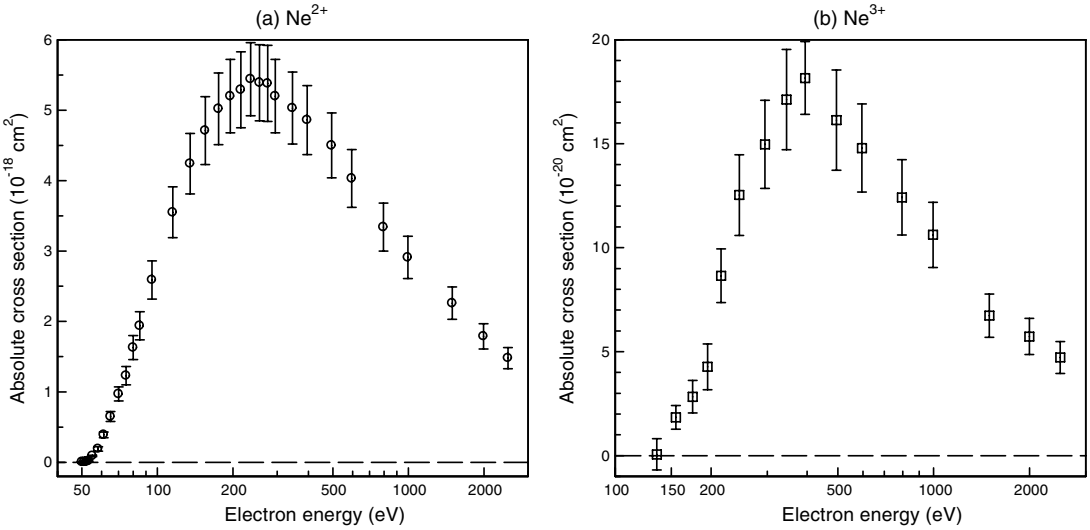

Figure 8. (a) Absolute cross sections for the production of Ne^{2+} (σ_4; ○), versus the electron energy. (b) Absolute cross sections for the production of Ne^{3+} (σ_5; □), versus the electron energy.

Table 4. Mean kinetic energy release values ($\overline{E_{KER}}$), for singly charged fragments, at indicated electron energies.

	E (eV)	15.1	21.1	25.1	45.1	95.1	295.1
DE	Ne^+	–	3.8 ± 0.4	–	–	–	–
	D^+	2.0 ± 0.3	–	2.2 ± 0.3	1.0 ± 0.2	1.2 ± 0.2	1.0 ± 0.2
DI	$Ne^+ + D^+$	–	–	–	5.9 ± 0.5[a]	8.9 ± 0.6[a]	9.0 ± 0.6[a]
					6.0 ± 0.4	6.8 ± 0.5	7.0 ± 0.5

[a] For DI: the upper $\overline{E_{KER}}$ values (upper line) are deduced from the Ne^+ measurements, whereas the lower one is obtained from the D^+ measurements.

for the ground state NeD^+. For each concerned excited molecular state, it is calculated as the difference between the energy defined by the corresponding potential energy curve and its dissociation limit. For dissociative excitation processes, the sum ($E_{KER} + D_0$) represents the energy lost by the incident electron. For dissociative ionization processes, the kinetic energy of the ejected electron being unknown, such an interpretation is not possible. In the experiment, it is unfeasible to distinguish the individual contribution of each concerned state and only the mean kinetic energy release ($\overline{E_{KER}}$) is estimated.

Kinetic energy release distributions are obtained for Ne^+ and D^+ (figures 7(a) and (b), respectively), at the electron energies where the magnetic scans were performed. For Ne^+, at the lowest incident electron energy (21.1 eV) which is below the dissociative ionization threshold, the KERD is due to dissociative excitation only. This distribution is seen to extend from 0 to 9 eV, below the theoretical KERs (∼8–10 eV), its mean kinetic energy release being estimated to be $\overline{E_{KER}} = 3.8 \pm 0.4$ eV (table 4). For D^+, KERDs exhibit a typical double peak shape that allows the separation of the dissociative excitation contribution (low E_{KER}, 0–3 eV) and of the DI one (high E_{KER}, 3–15 eV). For dissociative excitation, $\overline{E_{KER}}$ lies between 1.0 and 2.2 eV, again well below the calculated results (∼10–11 eV) (table 3). Thus, the low-energy KERDs may barely be attributed to the states $a^3\Sigma^+$, $b^3\Pi$, $d^3\Pi$ and $D^1\Pi$ for the Ne^+ production, or to the $c^3\Sigma^+$ and $C^1\Sigma^+$ states for the D^+ production. The above-mentioned indirect processes, implying the vibrational population and resonant capture, should be responsible for the low KER range of the distributions.

At high electron energies (95.1 eV and 295.1 eV), dissociative ionization dominates. The distributions, which broaden due to coulombic explosion, are seen to extend above 15 eV, both for Ne^+ and for D^+. Dissociation of the $X^2\Pi$ state, represented by the pure coulombic repulsive potential energy curve, predicts E_{KER} to be about 11.5 eV, which is comparable with the measured values (table 2).

Further theoretical investigations, including vibrational excitation of the parent ion and the subsequent broadening of the Franck–Condon region, should help to elucidate the problems pointed out by the present experiment in the discussion of the KERDs as well as of the energy thresholds.

4.4. Multiple ionization, formation of Ne^{2+} and Ne^{3+}

The cross sections (σ_4 and σ_5) corresponding to the Ne^{2+} and the Ne^{3+} formation are shown in figures 8(a) and (b), respectively. They are listed in table 5, together with the associated total uncertainties.

For Ne^{2+} formation, σ_4 is found to have a maximum value of $(5.4 \pm 0.5) \times 10^{-18}$ cm^2 at 235.1 eV and the appearance

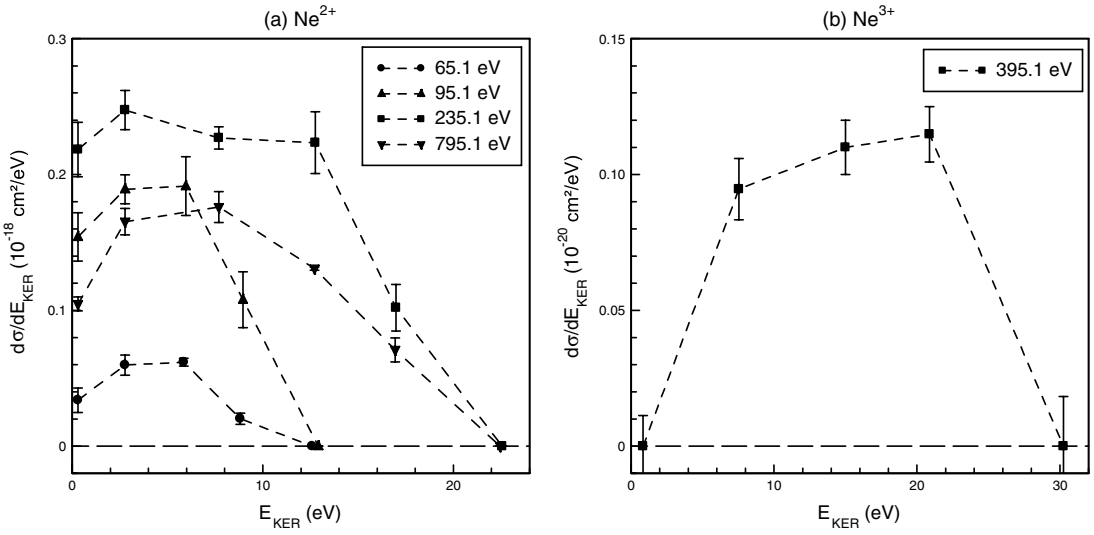

Figure 9. (a) Total kinetic energy release distributions for Ne^{2+} fragments, for indicated electron energies. (b) Total kinetic energy release distribution for Ne^{3+} fragments, for the indicated electron energy.

Table 5. Absolute cross sections for total production of Ne^{2+} and Ne^{3+} fragments (90% confidence limit).

	σ_4: Ne^{2+} (10^{-18} cm^2)		σ_5: Ne^{3+} (10^{-20} cm^2)	
E (eV)	σ_4	$\Delta\sigma_4$	σ_5	$\Delta\sigma_5$
50.1	0.006	0.006		
51.1	0.005	0.004		
52.1	0.01	0.01		
53.1	0.02	0.01		
55.1	0.09	0.01		
58.1	0.19	0.03		
61.1	0.39	0.04		
65.1	0.65	0.07		
70.1	1.0	0.1		
75.1	1.2	0.1		
80.1	1.6	0.2		
85.1	1.9	0.2		
95.1	2.6	0.3		
115.1	3.6	0.4		
135.1	4.2	0.4	0.1	0.8
155.1	4.7	0.5	1.8	0.6
175.1	5.0	0.5	2.8	0.8
195.1	5.2	0.5	4.3	1.1
215.1	5.3	0.5	8.7	1.3
235.1	5.4	0.5		
245.1			12.5	1.9
255.1	5.4	0.5		
275.1	5.4	0.5		
295.1	5.2	0.5	15.0	2.1
345.1	5.0	0.5	17.1	2.4
395.1	4.9	0.5	18.2	2.6
495.1	4.5	0.5	16.1	2.4
595.1	4.0	0.4	14.8	2.1
795.1	3.3	0.3	12.4	1.8
995.1	2.9	0.3	10.6	1.6
1495.1	2.3	0.2	6.7	1.0
1995.1	1.8	0.2	5.7	0.9
2495.1	1.5	0.2	4.7	0.8

energy is observed to be at (53.1 ± 0.5) eV. Below this ionization threshold, a weak signal ranging down to (50.1 ± 0.5) eV indicates the possible presence of vibrationally excited states in the primary beam up to $v < 10$, which is similar to what was previously observed for CO^+ (Lecointre *et al* 2006). The lowest energy for the Ne^{2+}+D dissociation limit is calculated to be 49.2 eV (Bashkin and Stoner 1975, Vasudevan 1975) so that, at the threshold, E_{KER} is estimated to be 3.9 eV. The lowest energy for the Ne^{2+}+D^+ dissociation limit (62.8 eV) is much higher than the observed threshold (53.1 eV). This indicates that the couple Ne^{2+}+D is favoured just above the Ne^{2+} appearance energy, the ion pair is thus produced less preferentially. At 65.1 eV (i.e., above the ion pair formation energy threshold), the KERD extends from 0 to 12 eV (figure 9(a)) and the associated $\overline{E_{KER}}$ is found to be (4.5 ± 0.5) eV, which is compatible with the estimated value (3.9 eV). At higher incident electron energies, due to coulombic explosion, the KERDs increase up to 22 eV and the largest $\overline{E_{KER}}$ is found to be (8.3 ± 0.7) eV at 795 eV.

For Ne^{3+} formation, σ_5 exhibits a maximum value of (18.2 ± 2.6) × 10^{-20} cm^2 at 395.1 eV and the appearance energy is found to be (132 ± 5) eV (figure 8(b)). The break observed around 200 eV is not identified; no excitation or ionization process can be invoked in this energy range. The energies for the dissociation limits Ne^{3+}+D and Ne^{3+}+D^+ are 112.6 eV and 126.2 eV, respectively (Bashkin and Stoner 1975, Vasudevan 1975). Therefore, the corresponding E_{KER}s are estimated to be around 19.4 eV and 5.8 eV, respectively. The presently determined KERD (observed only at 395 eV, figure 9(b)) extends up to 30 eV and the corresponding $\overline{E_{KER}}$ is calculated to be (15 ± 1) eV, which is compatible with 19.4 eV. This fact indicates that the couple Ne^{3+}+D is probably formed preferentially, rather than the Ne^{3+}+D^+ ion pair. The cross section σ_5 exhibits no evident distinctive shape indicating the presence of Auger processes associated with K-shell vacancy. For neon, the K–L excitation energy is 870.2 eV and the K-shell ionization energy is 914.6 eV (Bashkin and Stoner 1975).

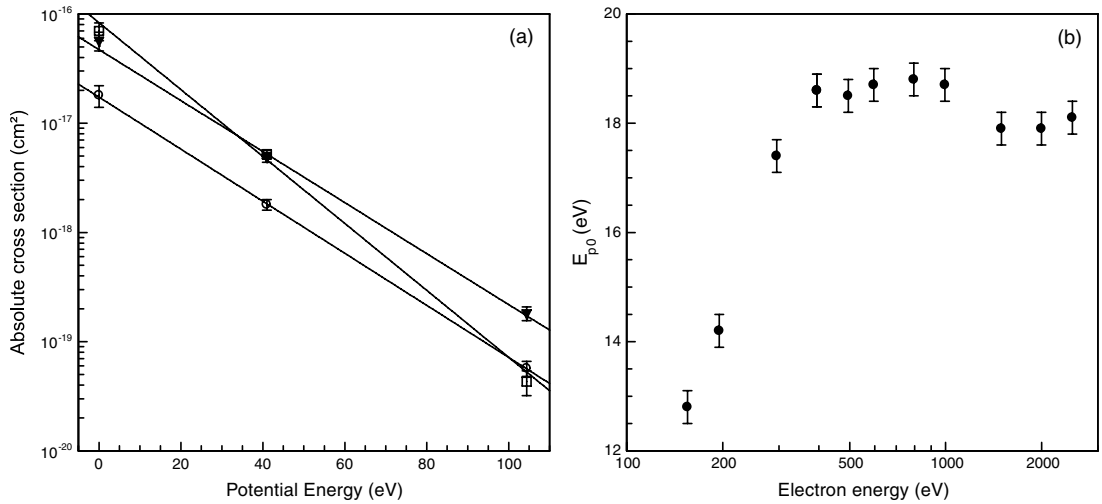

Figure 10. (a) Present absolute cross sections for individual ion pair (Ne^++D^+, Ne^{2+}+D^+ and Ne^{3+}+D^+), as a function of the corresponding potential energy at the dissociation limit, for several electron energies: (□) 195.1 eV ($\sigma_0 = 8.3 \times 10^{-17}$ cm^2; $E_{p0} = 14.2$ eV); (▼) 395.1 eV ($\sigma_0 = 4.7 \times 10^{-17}$cm^2; $E_{p0} = 18.6$ eV) and (○) 1995.1 eV ($\sigma_0 = 1.7 \times 10^{-17}$ cm^2; $E_{p0} = 18.2$ eV). The straight lines result from the fit by means of equation (20). (b) Parameter E_{p0} (●) as a function of the incident electron energy.

Attempts to observe Ne^{4+} formation were performed and the corresponding apparent cross section is found to be $(3.2 \pm 1.8) \times 10^{-21}$ cm^2 for an incident electron energy of 795 eV. Nevertheless, the signal was too weak to obtain the absolute cross section.

As observed previously for multiple ionization of CO^+ and CD^+ (Lecointre *et al* 2007a, 2007b), at a given electron energy, present ionization cross sections are seen (figure 10(a)) to reduce exponentially with the potential energy (E_p) of each dissociated ion pair, above the Ne^++D^+ dissociation limit, which is defined as the zero potential energy:

$$\sigma = \sigma_0 \exp(-E_p/E_{p0}), \tag{20}$$

σ_0 (10^{-17} cm^2) and E_{p0} (eV) are fitting parameters, the physical meaning of the latter being still unknown. In order to perceive its signification, it is useful to examine its dependence with the incident electron energy: E_{p0} is observed to rise from 13 eV to 19 eV for incident electron energies ranging from 155 eV up to 395 eV and, above 395 eV, it is kept almost constant (figure 10(b)). Theoretical investigations should bring expected enlightenments of both the meaning and the behaviour of this parameter.

5. Summary

Absolute cross sections for electron impact dissociative excitation and ionization of NeD^+, leading to the formation of ionic products (D^+, Ne^+, Ne^{2+} and Ne^{3+}) are reported in the energy range from their respective thresholds to 2.5 keV. Dissociative excitation leading to the D^+ formation is seen to dominate over the Ne^+ one. Present appearance energies of singly charged fragments are too low to be directly related to the lowest NeH^+ dissociative potential curves. The presence of vibrationally excited levels populated within the $X^1\Sigma^+$ ground state and the role of resonant NeH^{**} states may explain the observed thresholds. The resonant contribution is pointed out by subtraction of present results from the data of storage ring experiments (Novotny 2006). The resonant states lead to the formation of two neutral products (Ne+H), because no resonant signal is observed in the present experiment. The energy dependence of the electron impact ionization cross section can adequately be represented by the usual Bethe form above 60 eV. The analysis of the fragment velocity distributions allows the determination of the kinetic energy release for dissociation products, at selected electron energies. The potential energy curves are presented for the dissociation channels, which are of importance for the detailed discussion of present experimental results. This set of curves concerns the neutral molecule (also formed in Rydberg states), the singly and the doubly charged ions and it includes recent theoretical results of Ngassam *et al* (2007). At a given incident electron energy, the cross sections are seen to decrease exponentially with respect to the potential energy of each dissociated ion pair.

Acknowledgements

The authors acknowledge the financial support of the Association Euratom-Belgian State and the technical support of C Alaime and D Dedouaire. They gratefully thank A I Florescu-Mitchell for valuable discussion and they are indebted to the Forschungszentrum Jülich for the lending of the ECR ion source.

References

Abdellahi El Ghazaly M O, Jureta J J, Urbain X and Defrance P 2004 *J. Phys. B: At. Mol. Opt. Phys.* **37** 2467
Amitay Z, Zajfman D and Forck P 1994 *Phys. Rev.* A **50** 2304
Bahati E M, Jureta J J, Belic D S, Cherkani-Hassani H, Abdellahi M O and Defrance P 2001 *J. Phys. B: At. Mol. Opt. Phys.* **34** 2693

Bainbridge K T 1933 *Phys. Rev.* **43** 103
Bashkin S and Stoner J O Jr 1975 *Atomic Energy Levels & Grotrian Diagrams I, Hydrogen I–Phosphorus XV* (Amsterdam: North-Holland)
Berkowitz J 1971 *Chem. Phys. Lett.* **11** 21
Bondybey V, Pearson P K and Schaefer H F 1972 *J. Chem. Phys.* **57** 1123
Cherkani-Hassani H, Belic D S, Jureta J J and Defrance P 2006 *J. Phys. B: At. Mol. Opt. Phys.* **39** 5105
Defrance P, Brouillard F, Claeys W and Van Wassenhove G 1981 *J. Phys. B: At. Mol. Opt. Phys.* **14** 103
Florescu-Mitchell A I and Orel A E 2004 *6th Int. Conf. on Dissociative Recombination (Mosbach, Germany)*
Inokuti M 1971 *Rev. Mod. Phys.* **43** 297
Lecointre J, Belic D S, Cherkani-Hassani H, Jureta J J and Defrance P 2006 *J. Phys. B: At. Mol. Opt. Phys.* **39** 3275
Lecointre J, Belic D S, Jureta J J, Becker K, Deutsch H, Limtrakul J, Märk T D, Probst M and Defrance P 2007a *J. Phys. B: At. Mol. Opt. Phys.* **40** 85
Lecointre J, Cherkani-Hassani S, Belic D S, Jureta J J, Becker K, Deutsch H, Märk T D, Probst M, Janev R K and Defrance P 2007b *J. Phys. B: At. Mol. Opt. Phys.* **40** 2201
Lorenzen J, Hotop H, Ruf M W and Morgner 1980 *Z. Physik* A **297** 19
Lukanow H and Schuetze W 1933 *Z. Physik* **82** 610
Miller W F and Platzman R L 1957 *Proc. Phys. Soc.* A **70** 299
Mitchell J B A 1996 *Dissociative Recombination III: Theory, Experiment and Applications* ed D Zajfman, J B A Mitchell, D Schwalm and B R Rowe (Singapore: World Scientific) p 21
Mitchell J B A 2001 *Atomic and Plasma-Material Interaction for Fusion* vol 6 (Vienna: International Atomic Energy Agency) p 97
Mitchell J B A, Novotny O, Angelova G, LeGarrec J L, Rebrion-Rowe C, Svendsen A, Andersen L H, Florescu-Mitchell A I and Orel A E 2005 *J. Phys. B: At. Mol. Opt. Phys.* **38** 693
Ngassam V, Florescu-Mitchell A I and Orel A E 2008 *Phys. Rev.* A submitted
Novotny O 2006 *PhD Thesis*, Université de Rennes I
Petsalakis I D, Theodorakopoulos G, Li Y, Hirsch G, Buenker J and Child M S 1998 *J. Chem. Phys.* **108** 7607
Peyerimhoff S 1965 *J. Chem. Phys.* **43** 998
Rescigno T N, Lengsfield B H and McCurdy C W 1995a *Modern Electronic Structure Theory* vol 1ed D R Yarkony (Singapore: World Scientific) p 501
Rescigno T N, Orel A E, McCurdy C W and Lengsfield B H 1995b *Computational Methods for Electron-Molecule Collision* ed W M Huo and F A Gianturco (New York: Plenum)
Rich W B, Bobbio S M, Champion R L and Doverspike L D 1971 *Phys. Rev.* A **4** 2253
Rosmus P and Reinsch E-A 1980 *Z. Naturforsch.* A **35** 1066
Schopman J and Los J 1971 *Physica* **51** 132
Van der Wiel M J, El-Sherbini Th M and Vriens L 1969 *Physica* **42** 411
Vasudevan K 1975 *Mol. Phys.* **30** 437
Weise H P, Mittman H U and Henglein A 1971 *Z. Naturforsch.* **26a** 112
Wind H 1965 *J. Chem. Phys.* **43** 2956
Zhang T, Qian H M, Tang X N, Ng C Y, Chiu Y, Levandier D J, Miller J S and Dressler R A 2003 *J. Chem. Phys.* **119** 10175